Chemistry & Biology
Article

Structural and Functional Analysis of *Bacillus subtilis* YisP Reveals a Role of Its Product in Biofilm Production

Xinxin Feng,[1,6] Yumei Hu,[2,6] Yingying Zheng,[2,6] Wei Zhu,[1] Kai Li,[1] Chun-Hsiang Huang,[2] Tzu-Ping Ko,[3] Feifei Ren,[2] Hsiu-Chien Chan,[2] Mulugeta Nega,[4] Shannon Bogue,[1] Daniel López,[5] Roberto Kolter,[5] Friedrich Götz,[4] Rey-Ting Guo,[2,*] and Eric Oldfield[1,*]

[1]Department of Chemistry, University of Illinois, Urbana, IL 61801, USA
[2]Industrial Enzymes National Engineering Lab, Tianjin Institute of Industrial Biotechnology, Tianjin 300308, China
[3]Institute of Biological Chemistry, Academia Sinica, Taipei 11529, Taiwan
[4]Interfaculty Institute for Microbiology and Infection Medicine Tübingen, University of Tübingen, Tübingen 72076, Germany
[5]Department of Microbiology and Immunobiology, Harvard Medical School, Boston, MA 02115, USA
[6]Co-first author
*Correspondence: guo_rt@tib.cas.cn (R.-T.G.), eo@chad.scs.uiuc.edu (E.O.)
http://dx.doi.org/10.1016/j.chembiol.2014.08.018

SUMMARY

YisP is involved in biofilm formation in *Bacillus subtilis* and has been predicted to produce C30 isoprenoids. We determined the structure of YisP and observed that it adopts the same fold as squalene and dehydrosqualene synthases. However, the first aspartate-rich motif found in essentially all isoprenoid synthases is aspartate poor in YisP and cannot catalyze head-to-head condensation reactions. We find that YisP acts as a phosphatase, catalyzing formation of farnesol from farnesyl diphosphate, and that it is the first phosphatase to adopt the fold seen in the head-to-head prenyl synthases. Farnesol restores biofilm formation in a Δ*yisp* mutant and modifies lipid membrane structure similarly to the virulence factor staphyloxanthin. This work clarifies the role of YisP in biofilm formation and suggests an intriguing possibility that many of the YisP-like homologs found in other bacteria may also have interesting products and functions.

INTRODUCTION

There is currently considerable interest in the structure, function, and inhibition of the enzymes involved in isoprenoid biosynthesis since, in many instances, these enzymes represent new drug targets (Oldfield, 2010; Oldfield and Lin, 2012). One such class of molecules catalyze the "head-to-head" condensation of isoprenoid diphosphates to form triterpenes such as squalene and dehydrosqualene, reactions catalyzed by squalene synthase (SQS) and dehydrosqualene synthase (CrtM, in *Staphylococcus aureus*), respectively (Figure 1). Inhibition of SQS is of interest in the context of the development of cholesterol-lowering drugs (Kourounakis et al., 2011) and of antiparasitics targeting ergosterol biosynthesis (Shang et al., 2014; Urbina, 2009), while CrtM is of interest because in *S. aureus*, it is involved in formation of staphyloxanthin (Pelz et al., 2005; Wieland et al., 1994), a virulence factor for the organism providing resistance to killing from host reactive oxygen species (Clauditz et al., 2006; Liu et al., 2005). Interestingly, staphyloxanthin levels are elevated in *S. aureus* biofilms (Resch et al., 2005), and the CrtM inhibitor zaragozic acid (Figure 1B) inhibits biofilm formation by affecting lipid microdomain ("raft") organization (López and Kolter, 2010). An effect of staphyloxanthin on bacterial membrane structure (order) has been shown via fluorescence depolarization (of a 1,3,5-diphenylhexatriene probe), and cells with elevated staphyloxanthin level are more rigid and more resistant to the membrane-targeting antibiotic daptomycin (Mishra et al., 2011).

A close analog of the *crtM* gene (*yisP*) is also present in *Bacillus subtilis*, and it was recently reported (López and Kolter, 2010) that YisP was involved in biofilm and pigment formation in *B. subtilis* and had SQS activity. To learn more about the structure and function of YisP, we have solved its structure by X-ray crystallography and determined the structure of the product formed by YisP from farnesyl diphosphate (FPP), as well as its effect on biofilm formation, in *B. subtilis*.

The BsYisP sequence is shown in the alignment in Figure 2, and it appears on initial inspection to contain the two expected "aspartate-rich" (DDXXD/E and DXXXD) domains (Christianson, 2006) found in many prenyl transferases, with a DDLDE and DLGTD motif being found in the sequence. However, as can be seen in the alignment of YisP, CrtM, and SQS in Figure 2, there are some puzzling features. First, the region of the first aspartate-rich motif (FARM) seen in the alignments of many prenyl synthases, in YisP, is aspartate poor: AASAD. Second, the DDLDE motif is actually between the FARM and second aspartate-rich motif (SARM) found in human SQS (HsSQS) and CrtM. These results suggest either that YisP might not make squalene (or dehydrosqualene), because a DDXXD motif in the FARM region is expected to be involved in Mg^{2+} binding and allylic diphosphate ionization to initiate catalysis, or that it has an unusual fold that is not suggested by the sequence alignments.

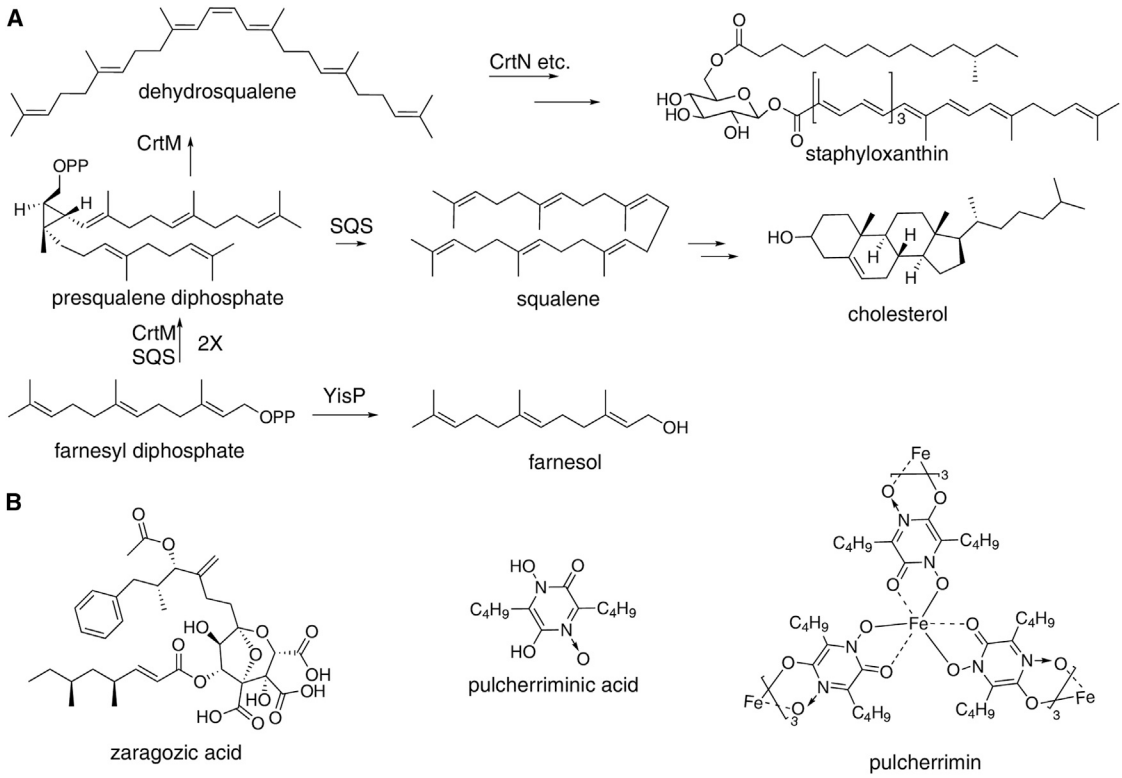

Figure 1. Structures of Compounds of Interest
(A) Biosynthesis of virulence factors, sterols, and farnesol.
(B) A biofilm inhibitor and some *B. subtilis* pigments.

RESULTS AND DISCUSSION

The Structure of *B. subtilis* YisP

In recent work (Hu et al., 2013) we cloned, expressed, purified, crystallized, and obtained diffraction data on *B. subtilis* YisP. The crystals belonged to the orthorhombic space group $P2_12_12_1$ with unit-cell parameters a = 43.966 Å, b = 77.576 Å, c = 91.378 Å, and diffracted to 1.92 Å. Here, we solved the YisP structure by using two Hg-containing derivatives (BsYisP has only 23% sequence identity with *S. aureus* CrtM, and the structure could not be solved by molecular replacement). Full data collection and refinement statistics are given in Table S1 (available online). We obtained one structure (Figure 3) with a molecule bound in the active site region, most likely a polyethylene glycol (PEG) from the crystallization buffer and not a bound substrate or product isoprenoid, because as can be seen in the electron density (Figure S1), there are no methyl substituents and no planar groups. Numerous attempts to obtain structures of YisP with FPP, S-*thiolo*-FPP, S-*thiolo*-geranylgeranyl diphosphate (GGPP), or farnesol ligands were unsuccessful.

The YisP molecule adopts the ε-fold as do CrtM and SQS (Figure 3A), but the DDLDE motif is located some 20 Å outside of the active site region found in the CrtM and SQS structures (Figure 4), while the AASAD motif superimposes on the first aspartate-rich motif found in these proteins, as does the second aspartate-rich motif. A possible implication of these results is that YisP might not function as a head-to-head prenyl synthase since the first aspartate residue found in CrtM and SQS is actually an alanine in YisP, and the DDLDE motif is well outside the active site region found in CrtM and SQS. There is one main pocket in the YisP structure, with a total volume (calculated using PocketFinder [Hendlich et al., 1997]) of ~1,000 $Å^3$. This pocket (Figure 3A, black mesh) is occupied by the single PEG molecule (Figure 3B), which is located in the S2 (prenyl donor) site identified previously in CrtM and SQS (Liu et al., 2008). Notably, this pocket volume is much smaller than that found in CrtM protein structures (~1,600 $Å^3$, on average; Figure 4A) or HsSQS (~1,900 $Å^3$, on average; Figure 4B), suggesting the possibility that the YisP product might be smaller than the C30 species produced by CrtM and SQS.

The Nature of YisP Activity: YisP Is a Phosphatase

We next sought evidence for formation of any head-to-head (squalene or squalene-like) condensation products since only phosphate release was detected in earlier work (López and Kolter, 2010). We carried out reactions with many combinations of diphosphates (including isopentenyl diphosphate [IPP], dimethylallyl diphosphate [DMAPP], geranyl diphosphate [GPP], FPP and GGPP) with Mg^{2+} or Mn^{2+} in the presence or absence of NADH or NADPH, but we found no evidence for condensation products (by radio-thin-layer chromatography [TLC] or by gas chromatography-mass spectrometry) under conditions where large amounts of squalene or dehydrosqualene were readily detected with SQS or CrtM. We also used several different

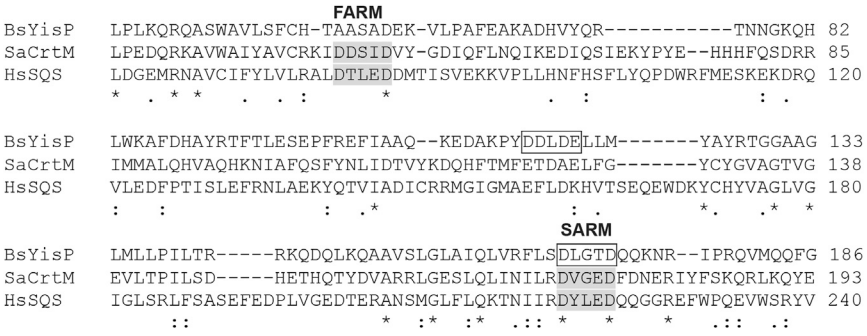

Figure 2. ClustalW Alignment of BsYisP, SaCrtM, and HsSQS Showing First and Second Aspartate-Rich Domains and the DDLDE Domain in BsYisP

detergents (Triton X-100, Tween 80, and IGEPAL), but we were again unable to detect any squalene or dehydrosqualene (or related) products. Nevertheless, consistent with earlier work, we did find that there was phosphate release using the preferred substrate (López and Kolter, 2010), FPP, as a substrate, but the reaction rate was only minimally affected by NADH or NADPH (Figure 5A). The product was, however, the sesquiterpene alcohol farnesol, as determined by radio-TLC using [^{14}C]FPP (produced from GPP and [^{14}C]IPP; Figure 5B). FPP reacted 2.5 times faster than did GPP and six times faster than did DMAPP, and GGPP was not active, in accord with results reported previously (López and Kolter, 2010). These results suggest that YisP may act as a phosphatase, not as a prenyl synthase.

Site-directed mutagenesis results showed that mutation of A54 and A55 in the AASAD motif to aspartate had only a small effect on phosphate-release activity (Figure S2), and again no condensation products were formed. However, D58A, D167A, and D171A mutants had only background levels of activity, Figure S2, indicating a role in catalysis. These results are consistent with the X-ray crystallographic result that the DDLDE motif is not in the active site region seen in CrtM or SQS, and the first aspartate in the DXXXD first aspartate-rich motif found in CrtM and SQS in YisP is an alanine. Mutations at this position in SQS are known to abrogate activity and in SQS, this aspartate is very highly conserved (Gu et al., 1998; Lin et al., 2010). Therefore, YisP adopts the ε-fold seen in SQS and CrtM but acts as a phosphatase, raising the question as to the origin of the pigmentation reported earlier (López and Kolter, 2010), in addition to the question of whether the YisP product effects biofilm formation.

B. subtilis Pigmentation

B. subtilis was reported in very early literature to not produce carotenoids (Clejan et al., 1986), consistent with our observation that YisP—the only head-to-head prenyl synthase-like enzyme in the *B. subtilis* genome—is a phosphatase. In *S. aureus*, the gene with direct homology to YisP is CrtM, which catalyzes formation of dehydrosqualene. *CrtM* is part of an operon—CrtMNOPQ—and the final product of this pathway is the bright orange carotenoid pigment, the virulence factor staphyloxanthin. However, in *B. subtilis*, it does not appear that *yisP* is part of an operon involved in carotenoid biosynthesis, with the adjacent genes being *yisA* (a DinB family, damage-inducible gene), *yisQ* (Norm, an Na^+-driven multidrug efflux pump), and *yisR* (an Arac family translational regulator). The issue is, then, the nature of the pigmentation seen in *B. subtilis*. As can be seen in Figure 5C, the UV-Vis spectra of both wild-type (WT) and a Δ*yisP* mutant strain of *B. subtilis* (at pH 7) are dominated by a broad peak with a λ_{max} of ~490 nm as well as a peak at 390 nm. The 490 nm peak is responsible for the dark red coloration of the cells (Figure 5C) and in previous work has been shown to arise from the complex formed between Fe^{3+} and pulcherriminic acid (Canale-Parola, 1963; Kupfer et al., 1967; Uffen and Canale-Parola, 1972) (Figure 1). The pigment was first identified in the yeast *Candida pulcherrima* and later in *B. subtilis* (Kluyver et al., 1953). On addition of base, the complex dissociates and sodium pulcherriminate (Figure 1) forms, with a λ_{max} = 410 nm (Kupfer et al., 1967). We thus find no evidence for squalene- or polyene-derived carotenoid pigments in *B. subtilis*, so earlier conclusions (López and Kolter, 2010) are hereby revised.

The Role of the YisP Product in Biofilm Formation and Its Effects on Lipid Bilayer Structure

We next investigated the possible effects of the YisP product detected here, farnesol, on *B. subtilis* biofilm formation. We used the Δ*yisP* mutant, which is unable to form biofilms and whose construction was reported earlier (López and Kolter, 2010), and as shown in Figure 6A, upon addition of farnesol, biofilm formation (on solid agar) is clearly visible (at right) in the Δ*yisP* mutant. Similar results were obtained in MSgg culture (Figure 6B) at 4 μM farnesol, and there were no effects on WT biofilm formation.

The issue then arises as to the likely role of farnesol in biofilm formation. In previous work, an important role for lipid microdomains in biofilm formation in *B. subtilis* (as well as *S. aureus*) was demonstrated (López and Kolter, 2010), so we hypothesized that farnesol might be involved since it is well known to affect lipid bilayer structure, as shown by both differential scanning calorimetry (DSC) and by solid-state deuterium nuclear magnetic resonance spectroscopy (Bondar et al., 1994; Funari et al., 2005; Rowat and Davis, 2004; Rowat et al., 2005). Specifically, farnesol shifts and broadens phospholipid gel-to-liquid crystal phase transitions and decreases ΔH, as does cholesterol (Ladbrooke et al., 1968; Oldfield and Chapman, 1972), and is involved in lipid microdomain (or raft) structures in eukaryotes, as illustrated in Figure 7A with 1,2-dihexadecanoyl-*sn*-glycerophosphoryl choline (DPPC). Interestingly, we find that staphyloxanthin also shifts and broadens the gel-to-liquid crystal phase transition and decreases ΔH (Figure 7A). The polyene in staphyloxanthin cannot be readily "bent," due to the presence of nine conjugated double bonds, in which case the molecule will act as a rigid body in the lipid bilayer (as does cholesterol) and its long/short side-chain structure suggests it may form an interdigitated structure (Figure 7B). This rigidifying effect of staphyloxanthin has been proposed (based on diphenylhexatriene fluorescence depolarization results) to "subvert non-oxidative host defenses mediated by cationic peptides" (Mishra et al., 2011) and could also block

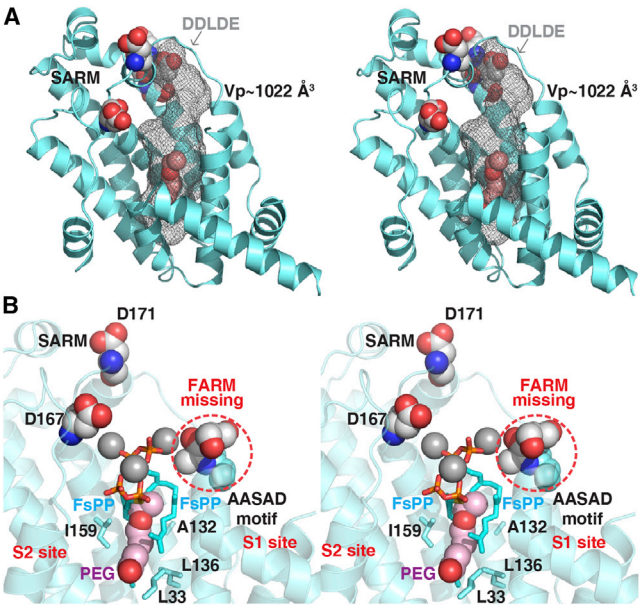

Figure 3. YisP Structures

(A) Stereo view of X-ray structure of YisP (Protein Data Bank [PDB] ID code 3WE9) showing the conserved SARM, the DDLED domain, and the ~1,000 Å^3 pocket.

(B) As in (A) but zoomed in to show the PEG ligand in S2, the SARM, and the location of the missing FARM. Structure superimposed on the two S-*thiolo*-FPP bound to CrtM (PDB ID code 2ZCP) showing PEG bound to YisP in S2 site. See also Figure S1 for electron density of the PEG ligand.

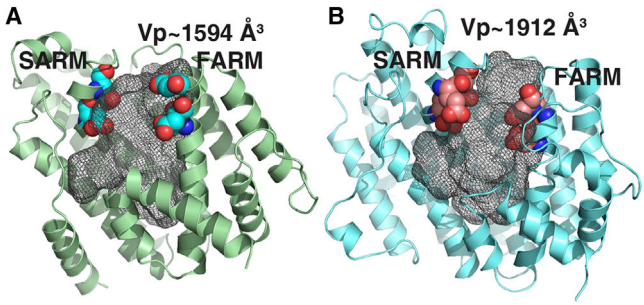

Figure 4. Crystal Structures of CrtM and SQS

(A) CrtM liganded structure (PDB ID code 3ADZ) showing (canonical) ~1,600 Å^3 pocket for S1+S2. The FARM and SARM are both conserved in the head-to-head prenyl synthases.

(B) HsSQS structure (PDB ID code 3LEE) showing larger pocket volume (~1,900 Å^3, on average) due to the need for NADPH to bind in SQS, but not CrtM. The smaller pocket in YisP suggests a smaller product than those produced by CrtM or SQS.

access of reactive oxygen species into *S. aureus*—an antivirulence effect—and changes in lipid microdomain structure also affect biofilm formation (López and Kolter, 2010).

SIGNIFICANCE

We report the X-ray structure of YisP from *B. subtilis*, known to be involved in biofilm formation. The fold is similar to that seen in *S. aureus* CrtM and HsSQS, but YisP acts as a phosphatase. There are two "DDXXD"-like motifs, as found in many prenyl synthases, but one motif is ~20 Å from the active site seen in SQS and CrtM. The first "aspartate-rich" motif found in these prenyl synthases is also aspartate poor in YisP (AASAD), so YisP is unable to catalyze the head-to-head condensation of isoprenoid diphosphates (to form species such as dehydrosqualene or squalene), and no such products were obtained. The only product found was farnesol, meaning that YisP can act as a phosphatase, and we found that farnesol restored biofilm formation in a Δ*yisp* mutant under both solid agar and liquid medium (MSgg) growth conditions. The lack of any polyene or carotenoid pigments in *B. subtilis* is consistent with the absence of CrtM-like activity in YisP and the X-ray structure, and the pink or reddish coloration seen (in both WT and the Δ*yisp* mutant) is due to the presence of the iron-containing pigment pulcherrimin. Overall, the results are significant because they help clarify the role of YisP in biofilm formation in *B. subtilis.* In addition, since there are also many other bacteria that harbor CrtM- or YisP-like homologs (based on sequence analyses and structure predictions), based on the results presented here and with *S. aureus* it seems likely that many of these bacteria will also have interesting products and functions since some of these organisms (e.g., *Mycobacterium tuberculosis*) do not produce carotenoids (or sterols), so the role of their CrtM- or YisP-like proteins remains to be discovered.

EXPERIMENTAL PROCEDURES

Crystallization and Data Collection for BsYisP

BsYisP was cloned, expressed, and purified as described previously (Hu et al., 2013). WT BsYisP was first crystallized by using the Grid Screen PEG/LiCl screen kit (Hampton Research) and the sitting-drop vapor diffusion method. The reservoir solution (no. C6) contained 1 M LiCl, 0.1 M bicine (pH 9), and 20% w/v PEG 6000. Better crystals were obtained by optimizing the crystallization condition to 1 M LiCl, 0.1 M bicine (pH 9), and 18%–20% w/v PEG 6000 at 25°C for 2 days. To prepare heavy-atom derivatives, the Hg-containing reagents of Heavy Atom Screen Hg (Hampton Research) were used. Cryoprotectant solutions (1 M LiCl, 0.1 M bicine [pH 9], 20% w/v PEG 6000, and 10% glycerol) containing 2 mM Hg derivatives were used for soaking the WT crystals for about 1 hr.

The X-ray diffraction data sets were collected at beamlines BL13B1 of the National Synchrotron Radiation Research Center (NSRRC) and processed by using the HKL2000 program (Otwinowski and Minor, 1997). Prior to structural refinement, 5% randomly selected reflections were set aside for calculating R_{free} as a monitor. The multiple isomorphous replacement (MIR) data sets of Hg-containing derivatives were collected at a wavelength of 0.97622 Å (BL13B1). Combination of data sets from different Hg-derivative crystals with the "native" data set from the WT crystal using SOLVE and RESOLVE (Adams et al., 2010) improved the figure of merit values from 0.24 to 0.41, the *Z* scores from 8.56 to 18.51, and the number of autobuilt amino acid residues up to 177. The best results were obtained using mersalyl acid and mercuric acetate derivatives. Statistics of the two Hg-derivative data sets and the MIR phasing are summarized in Table S1. The model and map were further improved by computational refinement using Refmac5 (Murshudov et al., 1997). Finally, a complete model (but missing residues 57–81) with most side chains was built using ARP/wARP (Langer et al., 2008). Structural refinements were carried out using CNS (Emsley and Cowtan, 2004) and Coot (Brünger et al., 1998). Data collection and refinement statistics are summarized in Table S1. All diagrams of protein structures were prepared by using PyMol (http://www.pymol.org/).

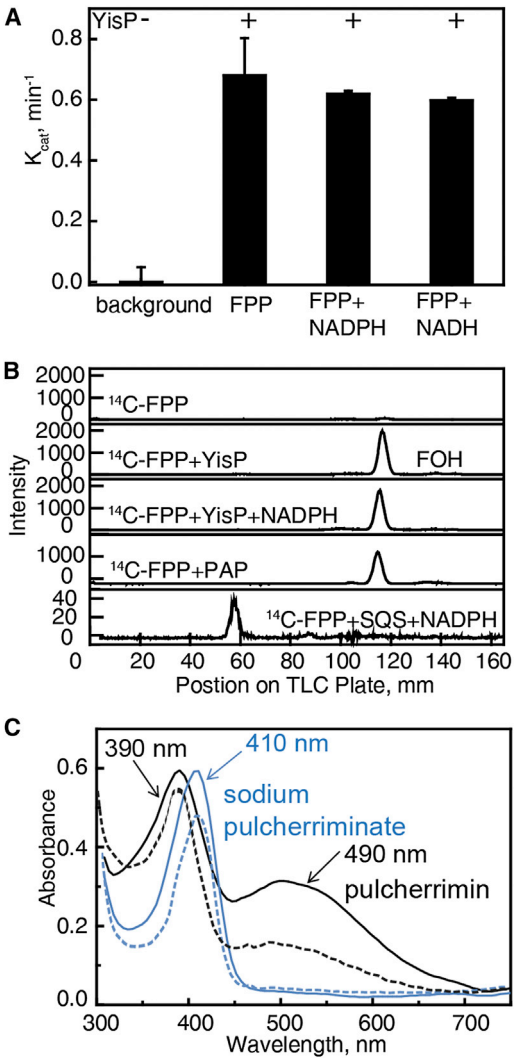

Figure 5. YisP Activity and Pigment Formation

(A) NADPH or NADH shows little effect on k_{cat} of YisP. Data are expressed as average ± SD of two independent experiments.

(B) FPP is converted to farnesol by YisP but to squalene by SQS in the presence of NADPH. The top trace is the control ([^{14}C]FPP, no YisP). PAP, potato acid phosphatase. See also Figure S2 for activities of WT and mutant YisPs.

(C) UV-Vis of *B. subtilis*. Cells produced a dark pink pigment (pulcherrimin, black lines). Upon addition of base the complex dissociates and sodium pulcherriminate forms (blue lines). WT cells are shown with solid lines, and Δ*yisP* mutant cells are shown with broken lines.

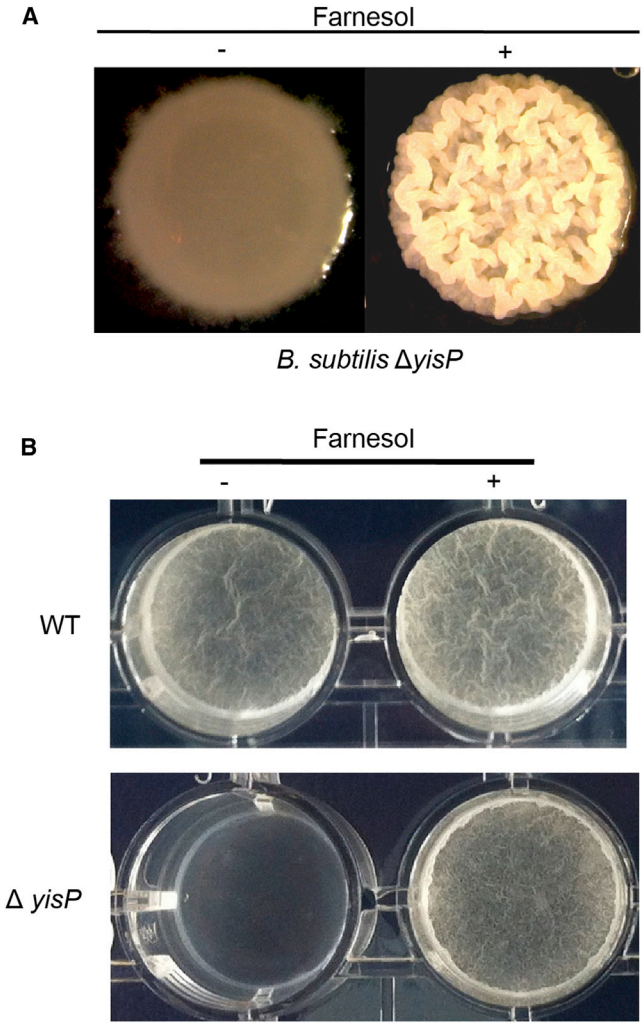

Figure 6. Biofilm Formation in *B. subtilis*

(A) Biofilm formation on solid agar requires the production of an extracellular matrix, which is correlated with the amount of wrinkles observed in the colony (López and Kolter, 2010). Treatment of the plate with a 10 μl drop of 500 μM farnesol restores biofilm formation in the Δ*yisP* mutant.

(B) Biofilm formation in *B. subtilis* WT and Δ*yisP* mutant, in the presence or absence of 4 μM farnesol.

Mutant Preparation

The mutants were prepared with a BsYisP–pET32 Xa/LIC vector as the template, and the following forward primers were used: 5′-GTATTG TCGTTTTGCCACACGGATGCCAGTGCAGACGAAAAGGTA-3′ for A54D, 5′-TGCCACACGGCGGCCAGTGCAGCGGAAAAGGTATTGCCCGCATTT′ for D58A, 5′-CAGCTGGTTCGCTTCTTAAGTGCGCTTGGCACAGATCAGCAA AAA-3′ for D167A, 5′-TTCTTAAGTGATCTTGGCACAGCGCAGCAAAAAAAC CGCATTCCC-3′ for D171A, and 5′-TTGTCGTTTTGCCACACGGATGATAG TGCAGACGAAAAGGTATTG-3′ for A54D/A55D. The recombinant plasmids were transformed to *Escherichia coli* BL21 trxB (DE3), and proteins were expressed and purified as for WT BsYisP (Hu et al., 2013).

BsYisP and HsSQS Activity Assay and Product Determination

The reaction of FPP catalyzed by BsYisP was monitored at 360 nm by using a continuous spectrophotometric assay (Webb, 1992) for diphosphate release in 96-well plates with 200 μl reaction mixtures containing 400 μM 7-methyl-6-thioguanosine, 0.1 U/ml purine nucleoside phosphorylase, and inorganic diphosphatase, 100 μM FPP, 100 μM NADPH or NADH, 25 mM Tris-HCl (pH 7.5), 0.2% detergent, and 1 mM $MgCl_2$. Detergents tested were Triton X-100, Tween 80, and IGEPAL, with IGEPAL giving the best activity.

Product identification of BsYisP and HsSQS was carried out using radio-TLC with ^{14}C-labeled FPP as substrate. The ^{14}C-labeled FPP was synthesized by adding 100 μM GPP, 100 μM [^{14}C]IPP, and 1 μM human farnesyl diphosphate synthase to 50 μl of 25 mM Tris-HCl (pH 7.5), 0.2% detergent, and 1 mM $MgCl_2$, and reacting at 37°C for 30 min. BsYisP or HsSQS (and 100 μM NADPH) was then added, and the resulting reaction mixture was incubated at 37°C for 2 hr. The reactions were then terminated by adding 500 μl of NaCl-saturated H_2O, and the product was extracted with *n*-hexane. The *n*-hexane solution was then concentrated and spotted onto a C18

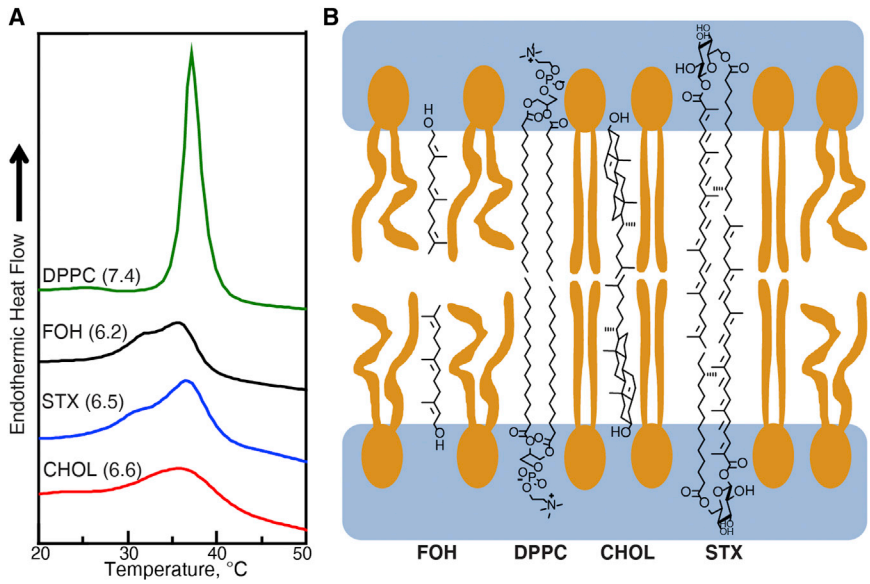

Figure 7. Effects of Virulence Factor and Raft Modulators on Lipid Bilayers

(A) DSC thermograms for DPPC (structure shown in B) in the presence of 20 mol % additives. The additives were farnesol (FOH), staphyloxanthin (STX), and cholesterol (CHOL). The numbers in parentheses are the ΔH for the main gel-to-liquid crystal phase transitions (in kcal/mole). Samples were in excess water.

(B) Cartoon showing proposed organization of virulence factor/raft modulators in membranes. The black stick DPPC structure serves as a "ruler" for CHOL, FOH, and STX. The orange cartoons represent ordered or disordered DPPC molecules.

reverse-phase TLC plate (Whatman). The TLC plate was developed with acetone/methanol (2:8), and the product distribution was analyzed by using a Storm 840 PhosphorImager and Quantity One (Bio-Rad).

Biofilm Formation Assay

Biofilm formation assays in *B. subtilis* were carried out as described previously (López and Kolter, 2010).

DSC

DPPC was obtained from Avanti Polar Lipids. Farnesol and cholesterol were obtained from Sigma-Aldrich. Staphyloxanthin was made as described previously (Nakano et al., 2011; Pelz et al., 2005); 20 mol % farnesol, cholesterol, or staphyloxanthin was codissolved with DPPC in chloroform. The organic solvent was removed under a stream of dry nitrogen, and the remaining solvent traces were removed in vacuo, overnight. Ten microliters of deionized water was added, and the mixtures were homogenized by hand. Weighed amounts of the mixtures were then sealed into solid sample inserts (stainless steel tubes). The DSC experiments were performed on a MicroCal VP-DSC instrument. The scans covered the range from 10°C to 60°C at a scan rate of 90°C/hr. The DSC thermograms were analyzed using Origin 7.1 (OrginLab). Water versus water scans were used for baseline correction.

ACCESSION NUMBERS

The PDB accession number for the YisP structure reported in this paper is 3WE9.

SUPPLEMENTAL INFORMATION

Supplemental Information includes two figures and one table can be found with this article online at http://dx.doi.org/10.1016/j.chembiol.2014.08.018.

AUTHOR CONTRIBUTIONS

X.F. carried out bioinformatics, enzyme activity, and product determination analyses. Y.H. and Y.Z. cloned, expressed, purified, crystallized, and solved the YisP X-ray structure. W.Z. performed DSC experiments. C.-H.H., T.-P.K., F.R., and H.-C.C. assisted with protein preparation and structure refinement. K.L. and S.B. assisted with assay development and pigment extraction. D.L. performed biofilm assays. M.N., F.G., R.K., and R.-T.G. provided input for experiment design. X.F. and E.O. wrote the paper with input from all authors.

ACKNOWLEDGMENTS

This work was supported by grants from the National High Technology Research and Development Program of China (2012AA022200), the National Basic Research Program of China (2011CBA00805 and 2011CB710800), the U.S. Public Health Service (NIH grant GM065307), a Harriet A. Harlin Professorship (E.O.), the University of Illinois/Oldfield Research Fund, and Deutsche Forschungsgemeinschaft (SFB766 to F.G.). X.F. was supported by a predoctoral fellowship from the American Heart Association, Midwest Affiliate (13PRE14510056). The synchrotron data collection was conducted on beamline BL13B1 of the NSRRC (Taiwan) supported by the National Science Council (Taiwan).

Received: July 8, 2014
Revised: August 14, 2014
Accepted: August 17, 2014
Published: October 9, 2014

REFERENCES

Adams, P.D., Afonine, P.V., Bunkóczi, G., Chen, V.B., Davis, I.W., Echols, N., Headd, J.J., Hung, L.-W., Kapral, G.J., Grosse-Kunstleve, R.W., et al. (2010). PHENIX: a comprehensive Python-based system for macromolecular structure solution. Acta Crystallogr. D Biol. Crystallogr. *66*, 213–221.

Bondar, O.P., Melnykovych, G., and Rowe, E.S. (1994). Effects of farnesol on the thermotropic behavior of dimyristoylphosphatidylcholine. Chem. Phys. Lipids *74*, 93–98.

Brünger, A.T., Adams, P.D., Clore, G.M., DeLano, W.L., Gros, P., Grosse-Kunstleve, R.W., Jiang, J.S., Kuszewski, J., Nilges, M., Pannu, N.S., et al. (1998). Crystallography & NMR system: A new software suite for macromolecular structure determination. Acta Crystallogr. D Biol. Crystallogr. *54*, 905–921.

Canale-Parola, E. (1963). A red pigment produced by aerobic sporeforming bacteria. Arch. Mikrobiol. *46*, 414–427.

Christianson, D.W. (2006). Structural biology and chemistry of the terpenoid cyclases. Chem. Rev. *106*, 3412–3442.

Clauditz, A., Resch, A., Wieland, K.P., Peschel, A., and Götz, F. (2006). Staphyloxanthin plays a role in the fitness of *Staphylococcus aureus* and its ability to cope with oxidative stress. Infect. Immun. *74*, 4950–4953.

Clejan, S., Krulwich, T.A., Mondrus, K.R., and Seto-Young, D. (1986). Membrane lipid composition of obligately and facultatively alkalophilic strains of *Bacillus* spp. J. Bacteriol. *168*, 334–340.

Emsley, P., and Cowtan, K. (2004). Coot: model-building tools for molecular graphics. Acta Crystallogr. D Biol. Crystallogr. *60*, 2126–2132.

Funari, S.S., Prades, J., Escribá, P.V., and Barceló, F. (2005). Farnesol and geranylgeraniol modulate the structural properties of phosphatidylethanolamine model membranes. Mol. Membr. Biol. *22*, 303–311.

Gu, P., Ishii, Y., Spencer, T.A., and Shechter, I. (1998). Function-structure studies and identification of three enzyme domains involved in the catalytic activity in rat hepatic squalene synthase. J. Biol. Chem. *273*, 12515–12525.

Hendlich, M., Rippmann, F., and Barnickel, G. (1997). LIGSITE: automatic and efficient detection of potential small molecule-binding sites in proteins. J. Mol. Graph. Model. *15*, 359–363, 389.

Hu, Y., Jia, S., Ren, F., Huang, C.H., Ko, T.P., Mitchell, D.A., Guo, R.T., and Zheng, Y. (2013). Crystallization and preliminary X-ray diffraction analysis of YisP protein from *Bacillus subtilis* subsp. *subtilis* strain 168. Acta Crystallogr. Sect. F Struct. Biol. Cryst. Commun. *69*, 77–79.

Kluyver, A.J., van der Walt, J.P., and van Triet, A.J. (1953). Pulcherrimin, the pigment of *Candida pulcherrima*. Proc. Natl. Acad. Sci. USA *39*, 583–593.

Kourounakis, A.P., Katselou, M.G., Matralis, A.N., Ladopoulou, E.M., and Bavavea, E. (2011). Squalene synthase inhibitors: An update on the search for new antihyperlipidemic and antiatherosclerotic agents. Curr. Med. Chem. *18*, 4418–4439.

Kupfer, D.G., Uffen, R.L., and Canale-Parola, E. (1967). The role of iron and molecular oxygen in pulcherrimin synthesis by bacteria. Arch. Mikrobiol. *56*, 9–21.

Ladbrooke, B.D., Williams, R.M., and Chapman, D. (1968). Studies on lecithin-cholesterol-water interactions by differential scanning calorimetry and X-ray diffraction. Biochim. Biophys. Acta *150*, 333–340.

Langer, G., Cohen, S.X., Lamzin, V.S., and Perrakis, A. (2008). Automated macromolecular model building for X-ray crystallography using ARP/wARP version 7. Nat. Protoc. *3*, 1171–1179.

Lin, F.Y., Liu, C.I., Liu, Y.L., Zhang, Y., Wang, K., Jeng, W.Y., Ko, T.P., Cao, R., Wang, A.H., and Oldfield, E. (2010). Mechanism of action and inhibition of dehydrosqualene synthase. Proc. Natl. Acad. Sci. USA *107*, 21337–21342.

Liu, G.Y., Essex, A., Buchanan, J.T., Datta, V., Hoffman, H.M., Bastian, J.F., Fierer, J., and Nizet, V. (2005). *Staphylococcus aureus* golden pigment impairs neutrophil killing and promotes virulence through its antioxidant activity. J. Exp. Med. *202*, 209–215.

Liu, C.I., Liu, G.Y., Song, Y., Yin, F., Hensler, M.E., Jeng, W.Y., Nizet, V., Wang, A.H., and Oldfield, E. (2008). A cholesterol biosynthesis inhibitor blocks *Staphylococcus aureus* virulence. Science *319*, 1391–1394.

López, D., and Kolter, R. (2010). Functional microdomains in bacterial membranes. Genes Dev. *24*, 1893–1902.

Mishra, N.N., Liu, G.Y., Yeaman, M.R., Nast, C.C., Proctor, R.A., McKinnell, J., and Bayer, A.S. (2011). Carotenoid-related alteration of cell membrane fluidity impacts *Staphylococcus aureus* susceptibility to host defense peptides. Antimicrob. Agents Chemother. *55*, 526–531.

Murshudov, G.N., Vagin, A.A., and Dodson, E.J. (1997). Refinement of macromolecular structures by the maximum-likelihood method. Acta Crystallogr. D Biol. Crystallogr. *53*, 240–255.

Nakano, C., Ootsuka, T., Takayama, K., Mitsui, T., Sato, T., and Hoshino, T. (2011). Characterization of the Rv3378c gene product, a new diterpene synthase for producing tuberculosinol and (*13R, S*)-isotuberculosinol (nosyberkol), from the *Mycobacterium tuberculosis* H37Rv genome. Biosci. Biotechnol. Biochem. *75*, 75–81.

Oldfield, E. (2010). Targeting isoprenoid biosynthesis for drug discovery: bench to bedside. Acc. Chem. Res. *43*, 1216–1226.

Oldfield, E., and Chapman, D. (1972). Dynamics of lipids in membranes: Heterogeneity and the role of cholesterol. FEBS Lett. *23*, 285–297.

Oldfield, E., and Lin, F.Y. (2012). Terpene biosynthesis: modularity rules. Angew. Chem. Int. Ed. Engl. *51*, 1124–1137.

Otwinowski, Z., and Minor, W. (1997). Processing of X-ray diffraction data collected in oscillation mode. Methods Enzymol. *276*, 307–326.

Pelz, A., Wieland, K.P., Putzbach, K., Hentschel, P., Albert, K., and Götz, F. (2005). Structure and biosynthesis of staphyloxanthin from *Staphylococcus aureus*. J. Biol. Chem. *280*, 32493–32498.

Resch, A., Rosenstein, R., Nerz, C., and Götz, F. (2005). Differential gene expression profiling of *Staphylococcus aureus* cultivated under biofilm and planktonic conditions. Appl. Environ. Microbiol. *71*, 2663–2676.

Rowat, A.C., and Davis, J.H. (2004). Farnesol-DMPC phase behaviour: a (2)H-NMR study. Biochim. Biophys. Acta *1661*, 178–187.

Rowat, A.C., Keller, D., and Ipsen, J.H. (2005). Effects of farnesol on the physical properties of DMPC membranes. Biochim. Biophys. Acta *1713*, 29–39.

Shang, N., Li, Q., Ko, T.-P., Chan, H.-C., Li, J., Zheng, Y., Huang, C.-H., Ren, F., Chen, C.-C., Zhu, Z., et al. (2014). Squalene synthase as a target for Chagas disease therapeutics. PLoS Pathog. *10*, e1004114–e1004114.

Uffen, R.L., and Canale-Parola, E. (1972). Synthesis of pulcherriminic acid by *Bacillus subtilis*. J. Bacteriol. *111*, 86–93.

Urbina, J.A. (2009). Ergosterol biosynthesis and drug development for Chagas disease. Mem. Inst. Oswaldo Cruz *104* (*Suppl 1*), 311–318.

Webb, M.R. (1992). A continuous spectrophotometric assay for inorganic phosphate and for measuring phosphate release kinetics in biological systems. Proc. Natl. Acad. Sci. USA *89*, 4884–4887.

Wieland, B., Feil, C., Gloria-Maercker, E., Thumm, G., Lechner, M., Bravo, J.M., Poralla, K., and Götz, F. (1994). Genetic and biochemical analyses of the biosynthesis of the yellow carotenoid 4,4′-diaponeurosporene of *Staphylococcus aureus*. J. Bacteriol. *176*, 7719–7726.